Image-Guided Analysis of Shoulder Pathologies: Modelling the 3D Deformation of the Subacromial Space during Arm Flexion and Abduction

Alexandra Branzan Albu[1], Denis Laurendeau[1], Luc. J. Hébert[2], Hélène Moffet[3], Marie Dufour[4], and Christian Moisan[4]

[1] Computer Vision and Systems Laboratory, Laval University, Québec (Qc) G1K 7P4, Canada
[2] Department of Radiology, Laval University, Québec(Qc), G1K7P4, Canada
[3] Department of Rehabilitation, Laval University, Québec(Qc), G1K7P4, Canada
[4]IMRI Unit, Québec City University Hospital, Québec (Qc) G1L 3L5, Canada

Abstract. This paper describes a simple, yet efficient method for modelling complex musculo-skeletal structures in motion. The proposed approach contains three main modules: segmentation, 3D reconstruction, and feature extraction. The segmentation module integrates region and edge information in a coherent manner. The 3D reconstruction technique is based on morphological morphing between adjacent slices and on contour-based extrapolation of extreme slices. Model validation is a rather challenging task, since no direct access is possible to *in vivo* human bony structures of the shoulder complex. We implement an internal validation approach, based on comparing the three models built for the same human shoulder. Finally, two descriptors of the subacromial space deformation during arm motion are computed. Their reliability is assessed using statistics of the healthy human shoulder.

1 Introduction

The painful shoulder is one of the most common musculo-skeletal complaints, and without an accurate diagnosis and treatment it may result in functional loss and disability. The successful evaluation of shoulder pain is rather complex and it relies on a hierarchical scheme for differential diagnosis [1]. Motion plays an important role in the evaluation process, which is either performed directly by the physical therapist or based on medical imaging techniques. Thus, physical examination is primarily based on the assessment of the active range of motion (ROM) and uses combinations of two basic motions: abduction and flexion. While standard protocols of clinical evaluation perform well in diagnosing shoulder instability, magnetic resonance (MR) exams are used for diagnosing the shoulder impingement syndrome [1].

The recent developments in the technology of MR image acquisition systems have opened interesting opportunities for the study of shoulder pathologies as well as for the assessment of the rehabilitation process. Specifically, the open-field architectures

with horizontal and vertical access allow for scanning the shoulder complex in different key positions during arm flexion and abduction. Whereas the study of the sub-acromial space deformations from MR images has recently provided promising results in [4], only static information was processed for the extraction of relevant features. Motion is an essential cue in the painful shoulder diagnosis. Most of the previous research about dynamic shoulder modelling is based on heavy kynematic constraints [2][3]. Moreover, the variation of inter-structural distances observed in MR images is difficult to integrate in kynematic models.

This paper proposes a new image-based modelling approach for the analysis of the subacromial space deformation during arm elevation and abduction. The organization of the rest of the paper is as follows. Section 2 presents the segmentation of MR image sequences, followed by the 3D reconstruction approach. Section 3 validates the reconstruction results, while section 4 describes the extraction of relevant features for describing shoulder motion. Finally, we draw the conclusions and describe future work.

2 Segmentation and 3D reconstruction

2.1 Semi-automatic segmentation approach

Prior to the 3D reconstruction of the anatomical structures from 2D image sequences, a segmentation step is necessary to identify the regions of interest corresponding to the bony structures. Our approach is task-oriented and well-adapted to particular aspects of MR shoulder images such as: a) the global appearance of the bony structures, which varies significantly in different planes (see Fig. 1a); b) the smooth structure-background transition, resulting in blurred boundaries of the ROI; c) the significant inter-slice variance of the average brightness during the same MR sequence; d) the complex morphology of the bony structures, not suitable for 3D segmentation, since the number of ROIs may vary from one slice to the next.

The database contains three types of parallel planar image sequences corresponding to three orthogonal orientations: saggital, axial and coronal (see Fig. 1a). Due to the significant length of the image sequences, a minimal user intervention in segmentation is desirable. A user-friendly interface is designed for the selection of a rectangular frame. This interface allows the user to scan the entire sequence at the desired speed, to pause for a thorough image examination and finally to draw a 2D rectangular region framing the structures of interest throughout the sequence. The frame is drawn only on one image and automatically mapped on all images in the same sequence.

Our segmentation method combines edge detection and region growing. First, the gradient image is computed with Sobel convolution masks. While low-magnitude edges are due to noise, high-magnitude edges are more likely to correspond, at least partially, to the contours of the bony structures. High-magnitude edges are selected by thresholding the edge image with the average value of the gradient magnitude, computed over the current image. The contours in the resulting binary image are not

closed (see Fig. 1b), due to local disconnections generated by the partial volume effect. Thus, a second segmentation step is necessary. This step consists in iterative pixel aggregation and uses the contour information to specify the similarity measure for candidate inclusion. Seed specification is automatic and histogram-based. Considering the global intensity histogram of the ROI, the seeds have intensity values belonging to the 5% inferior range of the histogram. As shown in Fig. 1c, most of the seed pixels are distributed in small labelled regions.

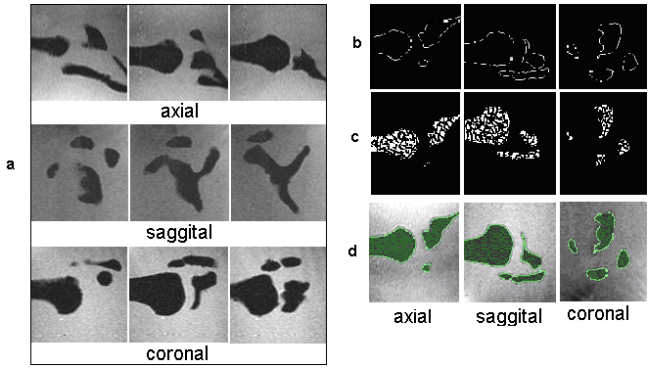

Figure 1. a) relevant samples of MR shoulder images corresponding to three standard orthogonal views b) edge image; c) seed regions for pixel aggregation; d) final segmentation

For every labelled growing region R_n, a corresponding list L_n is created. This list L_n contains contour pixels belonging to the labelled region R_n as well non-contour pixels adjacent to R_n and to at least one contour pixel. After sorting the list, the similarity threshold is set to the median value in the list. This similarity measure is consistent with the intensity variation inside the bony structures. At each iteration, adjacent pixels to a growing region are aggregated if their intensity exceeds the similarity threshold. While parallel pixel aggregations are performed for every labeled region, region merging is allowed after each iteration. Finally, we obtain a pairwise correspondence between the bony structures present in the current image and the final regions resulting from segmentation (see Fig. 1d). The parallel region growing stops when no candidate for inclusion in any of the regions satisfies the similarity measure.

2.2 3D reconstruction

We propose a 3D reconstruction approach using shape-based interpolation and extrapolation (see Fig. 2). Interpolation insures a smooth transition between every two adjacent input shapes and is based on *morphological morphing and "splitting"*. After interpolation, a *closing surface* step is performed using a new contour-based extrapolation technique. Our approach allows a coherent integration of the "closing" and "morphing" sequences, and an adjustable uniform inter-slice resolution as well. We implement the same surface rendering technique as in [5]. After rendering, a size-preserving surface fairing approach is implemented in a modified version from [6].

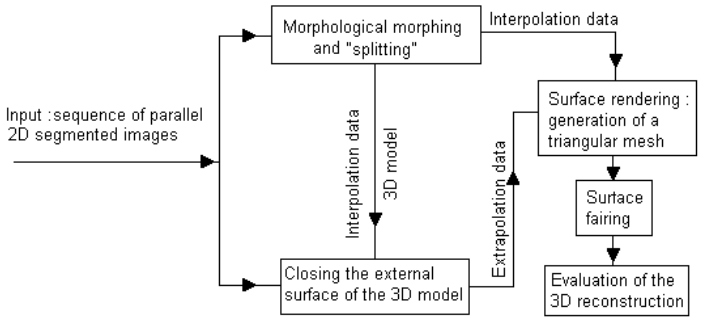

Figure 2. Diagram of the proposed 3D reconstruction algorithm

Morphological morphing of two simple compact regions. This morphing technique generates a gradual transition between two compact and partially overlapping shapes, as shown in Fig. 3. The mathematical formalism of this approach is described in [5]. While this technique works well for compact objects, the bony structures in the shoulder have a complex geometry leading to 'branching' situations.

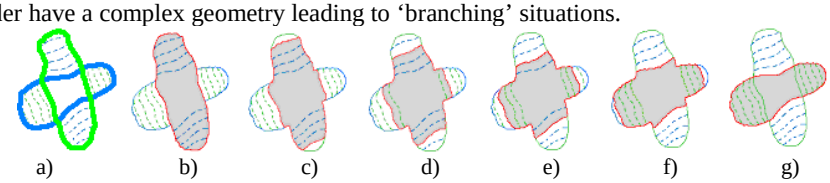

Figure 3. Morphing: a) superposition of the initial shape obj_1(green boundary) and the final shape obj_2 (blue boundary); the iterative conditional dilations of the common region with respect to obj_1 and of obj_2 are in dashed lines; b)initial shape in grey ; c), d), e), f) intermediate morphing iterations, resulting in grey objects with red boundaries; g) final shape(obj_2)

A morphological "splitting" approach A "branching" situation (see Fig. 4) occurs when two disjoint regions in slice *i* correspond to the same compact region in slice *i*+1. The idea is to divide the region resulting from "branch merging" into a sub-set of regions in order to allow a one-to-one correspondence. Instead of the classical solution using the Voronoi diagram [9], we propose a new morphological approach.

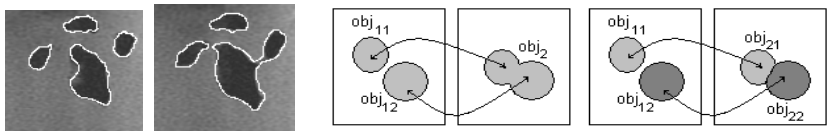

Figure 4. "Branching" in a shoulder MR sequence: a) four disjoint regions; b) merging of the previous right-most two regions into one region; c) inter-slice region correspondence before splitting; d) inter-slice region correspondence after splitting.

For simplicity, we consider the situation where two binary, disjoint, and compact objects obj_{11} and obj_{12} in slice 1 merge into one compact object obj_2 in slice 2. The "splitting" approach is to separate obj_2 into obj_{21} and obj_{22} as shown in Fig. 4 c and d. The main steps of the proposed "splitting" approach are as follows.

Step 1. Perform simultaneous and iterative non-conditional dilations on obj_{11} and obj_{12} obtaining $objd_{11}$ and $objd_{12}$ respectively, until $obj_2 \subseteq (objd_{11} \cup objd_{12})$. Since obj_{11} and obj_{12} are disjoint regions, and obj_2 is a compact region, it can be easily proven that $(objd_{11} \bigcap objd_{12}) \neq \Phi$. The morphological dilation operator is shape preserving, thus $objd_{11}$ and $objd_{12}$ preserve the shape of obj_{11} and obj_{12} respectively.

Step 2. Apply the watershed transform [9] to obj_2 and extract the watershed line *wshl* (i.e. the separation frontier between the regions detected with the watershed transform). As a result of "branch merging", obj_2 preserves to a given extent the shape of both initial "branches", obj_{11} and obj_{12}, thus the watershed transform is to generate the inter-slice one-to-one region correspondence. However, over-segmentation occurs when applying the watershed transform and must be eliminated in step 3.

Step 3. Extract the separation line *sep* that divides obj_2 in obj_{21} and obj_{22} :

$$sep = wshl \bigcap (objd_{11} \bigcap objd_{22})$$

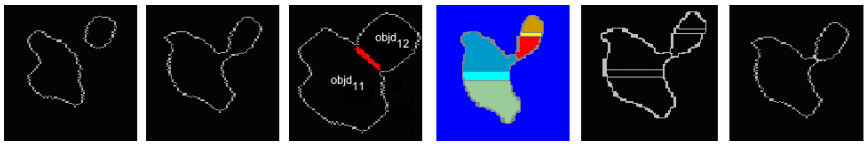

a b c d e f

Figure 5. The "splitting" approach : a) two "branches", obj_{11} and obj_{12}; b) object obj_2 resulting from the "merging" of the two "branches"; c) step 1 : $objd_{11} \bigcap objd_{22}$ is in red; d) step 2: over-segmentation of obj_2 in 6 classes (labeled with different colors) with the watershed transform ; e) step 2 : watershed line; f) step 3 : splitting obj_2 into obj_{21} and obj_{22}.

Fig. 5 illustrates the steps in the "splitting" approach. This technique may be easily extended to more than two disjoint "branches" merging into one compact region.

The surface closing step is implemented as a contour-based extrapolation, which is described in [5]. This step is necessary to correct the appearance of a cut-off cylinder of the 3D model resulting after the interpolation of parallel sequences.

3 Model Validation

The database for this study contains T1-weighted MR shoulder sequences from three orthogonal views: axial, sagittal and coronal, and corresponding to 6 human healthy subjects. The average length of a sequence is of 30 images. The images are stored in an uncompressed format and contain 256 gray levels. The size of the images is 256x256 pixels, while the intra-slice pixel resolution is of 1.25 mm. The value of slice thickness is set to 7 mm, which is a reasonable trade-off between the strength of the partial volume effect and the temporal extent of the acquisition process.

The reconstructed 3D shoulder model is to reproduce with high accuracy the real human bony structures at a 1:1 scale. Since a reference model is not available, we first perform an *internal validation* of our model. Specifically, for every human shoulder we build three models using the saggital, coronal, and axial sequences respectively. Next, we compare the models in order to assess their degree of similarity. If the models are quasi-identical, then the proposed 3D reconstruction method is robust and reliable. Model comparison is implemented in *Polyworks*, a software developed by Innovmetric Inc. and dedicated to the inspection of 3D models.
Error was computed in the region of interest, i.e. the structures surrounding the subacromial space (see Fig. 6a). A colour code allows us to visualize the spatial distribution of the error magnitude (see Fig. 6a). Green and light blue encode low magnitude values for positive and negative error respectively. For the case shown in Fig. 6a, the global error between the coronal and axial models is low, thus the models are considered quasi-identical. Table 1 centralizes information about inter-model comparison.

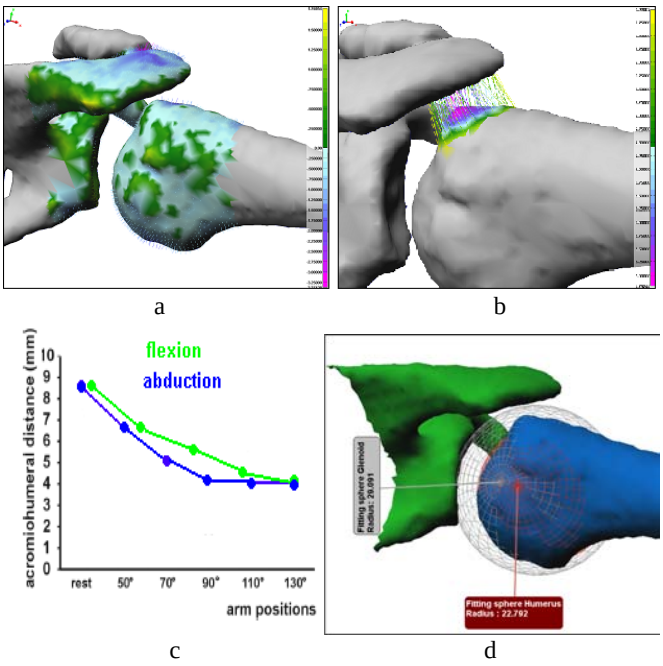

Figure 6. a) Model validation in *Polyworks*: a) comparing coronal and axial models corresponding to the same human shoulder b) computation of minimal acromio-humeral AHD distance c) temporal variation of AHD distance during arm flexion and abduction d) Relative position of the spheres matched on the humeral head and on the glenoid at rest.

Internal validation results in low-valued average errors for every human shoulder in the database. Therefore, the 3D models are reliable for the further computation of inter-structural distance measures. To verify the 1:1 scale factor of the 3D models, the minimal acromio-humeral distance (AHD) [4] is computed as shown in Fig. 6b. The

average AHD for the shoulders in our database is 6.0151, while the standard deviation is 0.659124. These values are coherent with statistical anatomical measures for healthy subjects.

Table 1. Results obtained after comparing of the coronal and axial models shown in Fig 6a.

Error distribution	
Model #1	Axial
Model#2	Coronal
#Points	5345
Mean error	-0.130989
StdDev	0.606965
Pts within +/-(1 * StdDev)	3758 (70.308700%)
Pts within +/-(2 * StdDev)	5118 (95.753040%)
Pts within +/-(3 * StdDev)	5317 (99.476146%)

4 Feature extraction

For the human shoulders in the database the acquisition process was performed at several key positions during arm elevation and abduction. Next, the AHD distance was computed. Fig. 6c illustrates the variation of the AHD distance with respect to the angle during arm flexion and abduction. The results show that the 3D AHD distance is more reliable than its 2D equivalent, which was measured manually by physical therapists on a graphical interface embedded in the acquisition system [4].
Moreover, since the glenoid cavity and the humeral head are in relative rotation during arm motion, we propose a new descriptor for assessing the dynamic surface compatibility of these two structures. In fact, if the convexity of the humeral head does not match the concavity of the glenoid cavity, or if their rotation is not concentric, then the sub-acromial space volume is reduced under a critical value, resulting in pressure on ligaments and tendons. Therefore, spheres are matched on each of the rotating surfaces. The matching algorithm minimizes the distance between the spherical surface and the reconstructed anatomical surface over the region of interest. Results are shown in Fig. 6d. For the healthy human shoulders in our database, the two spheres were almost concentric (average distance between centres was 2.178 mm), and the distance between the spherical centres was conserved during arm motion. Moreover, the average difference between the spherical radii (5.8 cm) represents a simple descriptor of the geometry of the subacromial space. Future work will continue to assess the reliability of spherical motion description for subjects with a painful shoulder.

5 Conclusions and future work

This paper presents a new end-to-end modeling technique for the study of the shoulder complex in motion. The input data consists of MR sequences acquired in three orthogonal planes and corresponding to key positions during arm flexion and abduction.

The output data contains 3D models of the shoulder complex in motion as well as descriptors of the subacromial space deformation.

The proposed modeling approach consists of three main modules: segmentation, 3D reconstruction, and feature extraction. The segmentation module integrates region and edge information in a coherent manner. Standard 3D reconstruction algorithms do not perform well on our input data, since the scanned volume is sampled in 7 mm-thick slices. Thus, we propose a new reconstruction technique based on morphological morphing between adjacent slices and on contour-based extrapolation of extreme slices. Model validation is difficult, since no direct access is possible to *in vivo* human bony structures of the shoulder complex. We implement an *internal validation* approach, based on comparing the three models built for the same human shoulder. Next, descriptors of the subacromial space deformation during arm motion are computed. The discrete temporal variation of the AHD distance is consistent with previous studies [4]. Moreover, we propose a descriptor for assessing the compatibility of two complementary surfaces, one concave and the other convex, during relative rotation.

While our modeling approach is task-oriented, it is easy to adapt it for the study of other joints, such as elbow, knee and ankle. Thus, we provide a simple, yet efficient method for modeling complex musculo-skeletal structures in motion.

Future work will focus on modeling motion as a continuous process. While MR acquisition will be performed only at discrete moments, temporal interpolation and view morphing [7] will allow for the continuous modeling of arm flexion and abduction. In addition, descriptors for assessing surface convexity and concavity, as well as for measuring local surface irregularities [8] will be tested for implementation.

References

1. van der Heijden GJ: Shoulder disorders: a state of the art review. Baillieres Best Pract Res Clin Rheumatol, 13(2), 1999,287-309

2. Engin, A. E., and Tumer, S. T.:Three-Dimensional Kinematic Modelling of the Human Shoulder Complex - Part I: Physical Model and Determination of Joint Sinus Cones", ASME Journal of Biomechanical Engineering, Vol. 111, 1989, 107-112.

3. Maurel, W. and Thalmann, D.: Human shoulder modelling including scapulo-thoracic constraint and joint sinus cones. Computer&Graphics, New York, vol.24(2), 1998, 203-218

4. Hébert, L.J., Moffet, H., Dufour, M., and Moisan,C.: Acromiohumeral distance in a seated position in persons with impingement syndrome. Journal of Magnetic Resonance Imaging, vol. 18(1), 2003, 72-79

5. Branzan-Albu, A., Schwartz, JM, Moisan, C., and Laurendeau, D.: Integrating geometric and biomechanical models of a liver tumour for cryosurgery simulation. Proc. of Surgery Simulation and soft Tissue Modeling IS4TM 2003, 121-131

6. Taubin G., "A signal processing approach to fair surface design", Computer Graphics, vol.29, 1995, 351-358.

7. Manning, A. and Dyer, R.C.: Interpolating view and scene motion by dynamic view morphing., Proc. of the IEEE Int. Conf. on Computer Vision and Pattern Recognition, 1999, 388-394.

8. Yushkevich, P., Pizer, S.M., Joshi, S., and Marron, J.S.: Intuitive, Localized Analysis of Shape Variability. Int. Conf. on Information Processing in Medical Imaging, 2001, 402-408.

9. Serra J.: Image Analysis and Mathematical Morphology. New York : Academic, 1982.